

Reducing suspension control noise with interferometric sensors—an experimental concept

N. L. Weickhardt¹ , A. Basalaev^{2,3} , O. Gerberding¹ 

¹ University of Hamburg, Institute of Experimental Physics, Luruper Chaussee 149, 22761 Hamburg

² Max Planck Institute for Gravitational Physics (Albert Einstein Institute), Callinstr. 38, Hannover, Germany

³ Institute for Gravitational Physics of the Leibniz Universität Hannover, Callinstr. 38, Hannover, Germany

E-mail: nils.weickhardt@uni-hamburg.de

July 2025

Abstract. One of the limiting noise sources of ground-based gravitational wave detectors at frequencies below 30 Hz is control-induced displacement noise. Compact laser interferometric sensors are a prime candidate for improved local displacement sensing. In this paper we present the design of an experiment that aims to demonstrate the advantages of interferometric sensors over shadow sensors. We mount two such interferometric sensors on two HAM Relay Triple Suspension (HRTS) systems that suspend two mirrors forming an optical cavity. As a model sensor we considered the compact balanced readout interferometer (COBRI), a sensor we are developing that is based on deep frequency modulation. By measuring the length stability of this cavity relative to a stable reference we aim to probe the direct motion reduction when using COBRIs for active damping and we aim to investigate their behavior and auxiliary functions, such as absolute ranging, in the context of the 6 degree-of-freedom controls of the suspensions. Here we describe the design of the experiment and simulations of the achievable noise levels that were obtained using mechanical models of the HRTS suspensions. We discuss all relevant noise sources, the modeled influence of the interferometric sensor damping and the current limitations and necessary improvements of our testing facility in terms of seismic pre-isolation to achieve a shadow sensor limited noise at around 5 Hz, where, according to our simulations, we can demonstrate superior performance for COBRIs in the longitudinal degree of freedom.

Keywords: mirror suspensions, interferometric displacement sensors, control systems, damping

1. Introduction

In 2015, the first direct detection [1] of a gravitational wave was achieved by the Advanced Laser Interferometer Gravitational-Wave Observatory (LIGO) [2] detectors, enabling us to observe the universe in a new way, complementary to electromagnetic radiation and astro-particles. Since then, many more gravitational waves originating

from compact binary inspiraling black holes and neutron stars have been detected [3, 4] by the LVK-Collaboration [5], a joint gravitational wave detector network formed by Advanced LIGO, Advanced Virgo [6] and KAGRA [7]. In one case [8], a binary neutron star merger was successfully detected together with its electromagnetic counterpart, demonstrating their importance to multi-messenger astronomy.

Increasing the sensitivity of these detectors at frequencies below 30 Hz would enable us to detect gravitational waves much earlier, from sources that are further away and with a higher signal-to-noise ratio. This would also lead to better sky localization, which is achieved through triangulation with multiple gravitational-wave detectors, aiding in the detection of particles and gamma rays that are also emitted by certain gravitational wave sources, such as merging neutron stars [8].

Gravitational-wave detectors are the most sensitive length difference measuring devices and are based on the Michelson interferometer [2]. They measure the differential arm length (DARM) of the interferometer, influenced by space-time curvature changes induced by a passing gravitational wave, causing relative length changes which are on the order of 10^{-21} . Therefore, it is necessary to isolate the interferometer optics from external forces. On Earth, one of the largest sources of noise is seismic motion, which can be decoupled from the test masses using suspensions. These suspensions provide isolation above their resonance frequencies, following an f^{-2n} behavior, where n denotes the number of pendulum stages, and f frequency, creating quasi-free test masses at high frequencies [9]. However, the test-mass motion is amplified at the resonance frequencies, resulting in significant total root-mean-square (RMS) motion. Meanwhile, current interferometers are designed to only operate in a narrow range of motion (\ll laser wavelength) where their response is approximately linear. Exceeding this range can lead to non-linear coupling and deteriorating control, and in the worst case, loss of lock and thereby reduced duty cycle, thus, an active damping system is typically used to reduce the test-mass motion at these resonances [10].

Such an active damping system requires a local displacement sensor to measure the pendulum motion and an actuator to counteract that motion. This is currently achieved with shadow sensors to measure the displacement and voice-coil setups for actuation [11, 12, 13]. However, since these sensors have a peak sensitivity of $1 - 0.04 \text{ nm}/\sqrt{\text{Hz}}$, depending on the frequency range and the exact variant, they introduce noise into the detector, limiting its performance at frequencies below 30 Hz [14]. While control loop shaping can be used to reduce this influence in the measurement band, this in turn limits the active damping as well, leading to a compromise in the design that is dominated by the sensor noise floor.

Improved local sensors with higher sensitivity would reduce control noise and decrease the RMS motion of the test masses, thereby increasing the sensitivity of the detector and its stability, as e.g. predicted for the Homodyne Quadrature Interferometer (HoQI) [15] at the future Big Beam-Splitter Suspension (BBSS) [16]. Such sensors are not only relevant to achieve the design sensitivities of current instruments, but are even more relevant for third-generation detectors like Cosmic Explorer (CE) [17] and the

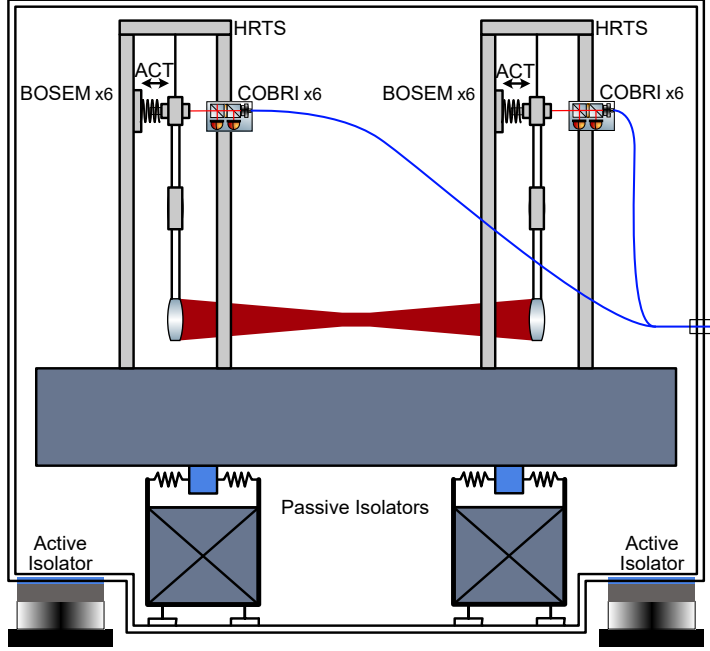


Figure 1. Sketch of the planned experimental setup. Two HRTS facing each other on a passively isolated optical table, inside VATIGrav, an actively isolated vacuum chamber. 6 DOF sensing and control at the top mass with both BOSEMs and COBRIs.

Einstein Telescope (ET) [18, 19]. Especially the latter aims for an improvement of about 6 orders of magnitude at 3 Hz in comparison to current detectors, which will be nearly impossible to realize with shadow sensors for local displacement sensing.

The sensor we are developing is the Compact Balanced Readout Interferometer (COBRI), which is based on ref. [20] and employs deep frequency modulation [21] to achieve multi-fringe sensing, absolute ranging, and a theoretical peak sensitivity of $10 \text{ fm}/\sqrt{\text{Hz}}$. In this paper, however, we simulated an experiment, which aims to show the improvement such sensors can have on the controls noise in suspensions.

2. Experimental setup

To study the assumed advantages and usability of interferometric sensors in a dedicated environment, we are designing an experiment using two HAM Relay Triple Suspension (HRTS) [22] systems, which will be used for LIGO [23, 24] and ET Pathfinder [25]. They were temporarily provided by the latter to us for the experiment described in this paper. The HRTS is a triple suspension with control of all six degrees of freedom (DOFs) using Birmingham Optical Sensors and Electro-Magnetic actuators (BOSEMs) [26] at the top mass, with a total pendulum length of 390 mm. OSEM generally measure displacement through shadow sensing. A flag attached to the top mass partially obstructs a light beam inside the OSEM. When the top mass moves, the amount of light passing by the flag changes, providing information about its displacement. For actuation, a magnet is attached to the flag. By passing a current through the coil wrapped around the outside

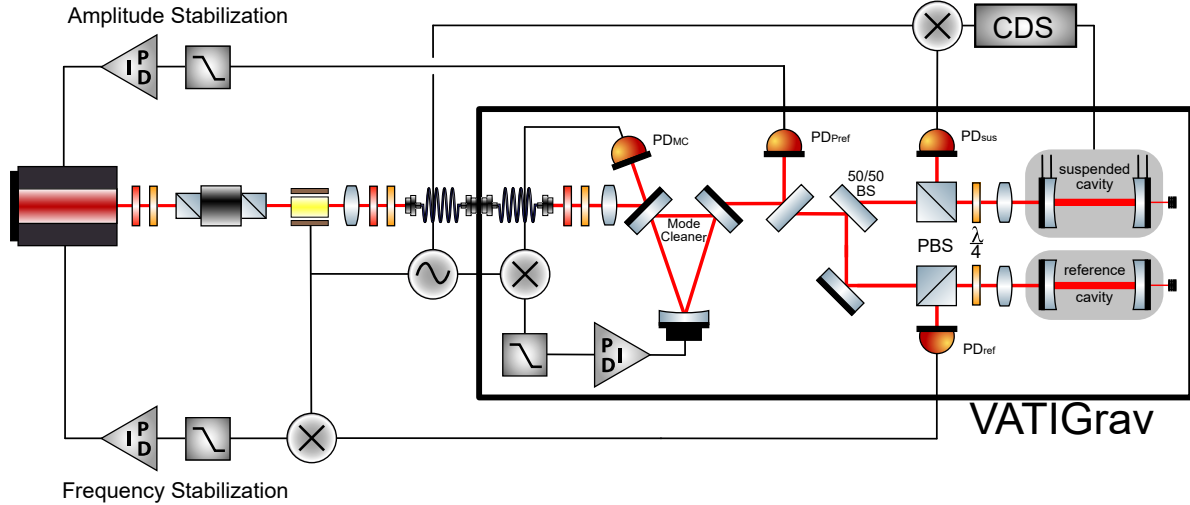


Figure 2. Proposed optical setup for the suspension cavity readout. The laser frequency stabilization is realized by locking the laser to a reference using PDH. The amplitude is stabilized via dc-offset locking with a power pick-off after the mode-cleaner in vacuum. The mode-cleaner is locked to the laser-frequency with PDH and the suspended cavity is kept on resonance with a digital control system, which also takes advantage of the PDH sidebands from locking to the reference cavity.

of the OSEM, a magnetic force is generated, which moves the flag and, consequently, the top mass. As depicted in Figure 1, we will mount a COBRI opposite each BOSEM, allowing us to switch from BOSEM sensing to COBRI sensing while still using the BOSEM coils for actuation, thus, allowing us to directly measure an improvement in suspension control. To reduce seismic noise, the experiment will be set up inside an actively isolated vacuum chamber (VATIGrav) [27] on an optical table, which rests on four passive isolators.

Measuring the improvement of control is accomplished using an optical resonator set up between the test masses of both HRTS systems, which will be read out using the Pound-Drever-Hall (PDH) technique [28], as shown in Figure 2 with design parameters in Table 1. To reduce coupling to laser frequency and amplitude noise, the laser needs to be locked to a monolithic reference cavity and stabilized in power. To minimize the effect of beam-jitter an input mode cleaner is introduced inside the vacuum chamber before coupling the laser into the cavities. Locking the mode cleaner will also be done with PDH by creating two sets of sidebands. One is being reflected by the mode cleaner to lock it, while the other set is transmitted by choosing a modulation frequency within the linewidth of the mode cleaner to lock to the reference cavity. The power stabilization will be done by introducing a pick-off behind the mode cleaner to account for power fluctuation that might be introduced by the electro optical modulator (EOM) or from the mode cleaner due to beam-jitter. Control of the suspended cavity is realized via digital system based on the LIGO Control and Data System (CDS) [29].

The vision goal of this experiment is to test any interferometric type displacement sensor [15, 30, 31, 32] using this setup, we, however, will focus on our COBRIs for the

Table 1. Design parameters of the proposed optical setup. These values are preliminary and are subject to change during the construction of the experiment.

Parameter	Symbol	Value
Laser wavelength	λ	1064 nm
Laser power	P_0	1 W
Mode cleaner Finesse	\mathcal{F}_{MC}	1000
Mode cleaner round-trip length	L_{MC}	53 cm
Mode cleaner FWHM	-	1 GHz
Suspended cavity Finesse	\mathcal{F}_{sus}	3140
Suspended cavity mirror separation	l_{sus}	40 cm
Reference cavity Finesse	\mathcal{F}_{ref}	3140
Reference cavity mirror separation	l_{ref}	20 cm

results shown in this paper and the initial stages of the experiment. Hence we will only refer to it in the following.

3. Suspension control modeling and noise discussion

Making assumptions about the motion of the cavity mirrors requires a set of simulation tools. One tool used is the Mathematica model for advanced LIGO suspensions [33], from which a state-space model can be exported that describes the mechanical properties of the suspension. This model is then read into the `spicycipy` [34] python package, based on Python Control Systems Library [35] and `GWpy` [36] packages, to compute frequency- and time-series responses of the suspension masses for various inputs, as well as to model the influence of control loops. All ASD plots presented here, unless explicitly indicated, are also calculated with `spicycipy` and the Logarithmic Power Spectrum Density (LPSD) algorithm [37], originally implemented in `LTPDA` package for the LISA mission [38].

In the following, we will denote transfer functions as P , the subscripts, e.g., on P_{x_0, x_3} , specify the displacement input (x_0 : suspension point in x -direction) to the displacement output (x_3 : test-mass in x -direction), where x is the direction along the cavity axis. In the case of force inputs F_{x_i} , the susceptibility, i.e. the force response of the mechanical system, is given by $P_{F_{x_i}, x_i}$, where i denotes one of the three masses of the pendulum suspension.

The noise contribution of each sensor to the test-mass motion in the x -direction \tilde{D}_{S, x_3} can be calculated with

$$\tilde{D}_{S, x_3} = \tilde{d}_S \cdot P_{F_{x_1}, x_3} \cdot \frac{G_o}{1 + G_o} \quad (1)$$

where \tilde{d}_S is the amplitude spectral density (ASD) of the sensor noise, $P_{F_{x_1}, x_3}$ is the susceptibility from a force input at F_{x_1} to a displacement output at x_3 and G_o the open-loop transfer function, which is given by

$$G_o = C_x \cdot P_{F_{x_1}, x_1} \quad (2)$$

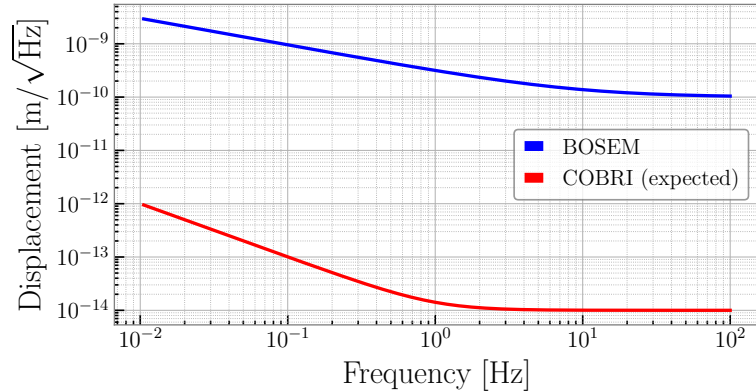


Figure 3. Amplitude spectral density models of the BOSEM- and expected COBRI sensing noise. The COBRI noise is dominated by laser frequency noise at low frequencies and electronic readout noise at high frequencies.

with the damping filter C_x and the susceptibility of the top mass $P_{F_{x_1},x_1}$. The damping filters we use for our analysis were published by Jeffrey Kissel in the SWG LIGO Logbook [39] and are designed to work for all DOFs on most suspensions. However, more optimal filters can be designed when interferometric sensors are used, which is an ongoing field of study [40] and beyond the scope of this paper. It should be noted that we plan to use more optimized filters after the initial phases of this experiment. Sensors with a higher sensitivity allow for more aggressive filtering without causing instabilities in the control loop and without introducing excess noise in the measurement band, since less noise will couple into it. This would increase the stability of the whole system and potentially result in an improved demonstration of the benefit interferometric displacement sensors have for the observatories.

The sensor noise models used for the BOSEM are taken from [26, 41], while the one for the COBRI is an estimation based on calculations of the Cramér-Rao lower bound [42], exhibiting a rising slope of f^{-1} toward lower frequencies to account for a limited suppression of laser frequency noise [43]. A similar noise performance using a single component DFMI-type sensor was previously achieved in ref. [44]. Both noise curves are shown in Figure 3.

The current seismic motion of the table inside VATIGrav was measured, with active isolation engaged, for both translations and rotations. The translational seismic motion was measured using a Trillium Horizon 120 (TH120) [45] seismometer, while rotations were measured using a Blueseis-3A [46] rotational seismometer and three TH120s set up in a triangular configuration. TH120 are conventional seismometers, relying on a proof mass to detect inertial motion, while Blueseis-3A is a fiber-optic gyroscope. Unlike a conventional seismometer, it features flat frequency response (in velocity). The results of these measurements are shown in Figure 4 and Figure 5, respectively. The rotational measurement indicates the noise floor of the Blueseis at $3 \times 10^{-8} \text{ rad s}^{-1}$ for frequencies above 1.5 Hz, while the triangular setup of the TH120s is sensitive to signals below that.

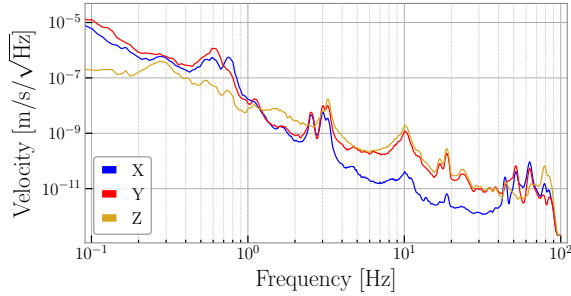


Figure 4. ASD of the seismic measurements in translation on the optical table with active and passive pre-isolation.

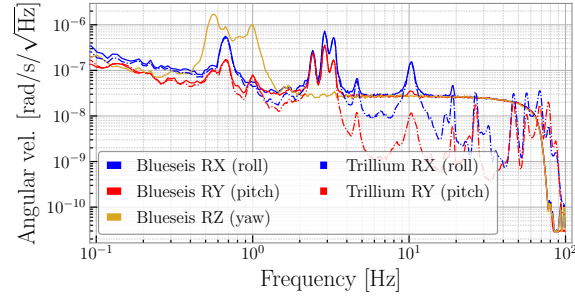


Figure 5. ASD of the seismic measurements in rotation on the optical table with active and passive pre-isolation.

However, despite the TH120s accurately resolving the features also measured by the Bluseis-3A, caution should be exercised in interpreting these results. The frequency response of TH120s is slightly different for each individual instrument and calibration is potentially sensitive to small changes in offsets from the ideal triangle as well as precise vertical alignment of each device. Therefore, data from triangular setup of the TH120s are not used for the simulations presented here.

An important source of noise for a controlled suspension is actuator noise, which we assumed is dominated by Digital-to-Analogue Converter (DAC) noise. We estimate it by assuming a white DAC noise of $5 \times 10^{-6} \text{ V}/\sqrt{\text{Hz}}$, for a DAC range of $\pm 10 \text{ V}$, which corresponds to a supplied current noise to the BOSEM coils of $\tilde{I}_d = 5 \times 10^{-9} \text{ A}/\sqrt{\text{Hz}}$. The actuator noise, denoted as \tilde{D}_a , is then given by

$$\tilde{D}_a = \tilde{I}_d \cdot c_F \cdot P_{F_{x_1,x_3}} \quad (3)$$

with the force constant $c_F = 0.12 \text{ N A}^{-1}$ [24] and the susceptibility $P_{F_{x_1,x_3}}$, converting the resulting force noise to a displacement of the test-mass.

One of the fundamental limitations will be suspension thermal noise, arising from Brownian motion and described by the Fluctuation-dissipation theorem [47]. It was calculated using the Mathematica models. However, the calculation of the thermal noise compared to the real-world system differs in one respect; for the blade springs, the material properties of steel were used instead of stainless steel, as the required properties had not been measured and were therefore not available to us. However, since the thermal noise at high frequencies is dominated by the contribution of the last stage wires [48], this discrepancy is expected to be negligible.

Similarly the coating thermal noise of the cavity mirrors arises from the same principle and its power spectral density (PSD) can be calculated with [49, 50]

$$S_{xx}(f) = \frac{2k_B T}{\pi^2 f} \frac{1}{w^2} \frac{1 - \sigma_{\text{sub}} - 2\sigma_{\text{sub}}^2}{Y_{\text{sub}}} \sum_j b_j d_j \phi_j \quad (4)$$

where k_B is the Boltzmann constant, $T = 293.15 \text{ K}$ the temperature, $\omega = 300 \mu\text{m}$ the waist radius, $\sigma_{\text{sub}} = 0.206$ and $Y_{\text{sub}} = 82 \text{ GPa}$ are the Poisson ratio and Young's modulus

of the substrate (N-BK7) [51]. d_j and ϕ_j are the thicknesses and mechanical losses of each coating layer made of tantalum (Ta_2O_5) and silica (SiO_2), which are $d_{\text{Ta}_2\text{O}_5} = 236 \text{ nm}$, $d_{\text{SiO}_2} = 347 \text{ nm}$, $\phi_{\text{Ta}_2\text{O}_5} = 3.8 \times 10^{-4}$ and $\phi_{\text{SiO}_2} = 0.4 \times 10^{-4}$. For the cavity mirrors used in this experiment we assume a 20 layer coating. b_j is a weighting factor and is given by

$$b_j = \left[\frac{(1 - 2\sigma_j)(1 + \sigma_j)}{(1 - 2\sigma_s)(1 + \sigma_s)} \right] \frac{1}{1 - \sigma_j} \times \left[\left(1 - n_j \frac{\partial \theta_c}{\partial \theta_j} \right)^2 \frac{Y_s}{Y_j} + \frac{(1 - \sigma_s - 2\sigma_s^2)}{(1 + \sigma_j)^2(1 - 2\sigma_j)} \frac{Y_j}{Y_s} \right] \quad (5)$$

where σ_j and σ_s are the Poisson's ratios of each coating and the substrate, n_j the reflective index of each layer and $\partial \theta_c / \partial \theta_j$ is the sensitivity of the total coating phase $\partial \theta_c$ to fluctuations in the round-trip phase $\partial \theta_j$ in the layers. This expression can be simplified by assuming the the substrate and coating elastic layers are equal ($Y_j \rightarrow Y_s$ and $\sigma_j \rightarrow \sigma_s$), and ignoring field penetration into the coating ($\partial \theta_c / \partial \theta_j \rightarrow 0$), $b_j \rightarrow 2$ for all layers.

Another fundamental noise source in the experiment is quantum noise, a combination of shot and radiation pressure noise, which arises from the power fluctuation of the laser due to shot noise. The displacement noise from shot noise is given by [52]

$$\tilde{D}_s = \frac{\sqrt{hc\lambda}}{8\mathcal{F}_{\text{sus}}\sqrt{P_c}} \quad (6)$$

with a carrier power of $P_c = 100 \text{ mW}$ at $\lambda = 1064 \text{ nm}$ and a finesse of the suspended cavity of $\mathcal{F}_{\text{sus}} = 3140$. The noise contribution, as ASD, due to radiation pressure can be calculated using

$$s_{xx}(f) = \frac{2\sqrt{\frac{2hcP_c}{\lambda}}}{c(1 - R)} \cdot P_{F_{x_3,x_3}} \quad [\text{m}/\sqrt{\text{Hz}}] \quad (7)$$

with the power reflectivity of the cavity mirrors $R = 0.999$ and the susceptibility $P_{F_{x_3,x_3}}$ to convert from force to displacement.

The last source of noise we took into consideration is frequency noise \tilde{f} originating, ideally, only from the length fluctuations \tilde{l}_{ref} of the reference cavity the laser will be locked to. It is calculated by

$$\tilde{f} = \frac{\tilde{l}_{\text{ref}}}{l_{\text{ref}}} \cdot f_0 \quad (8)$$

with the laser frequency f_0 and the reference cavity length l_{ref} . We assumed that the length fluctuations are dominated by a combination of coating thermal noise of the reference cavity mirrors and shot noise (radiation pressure noise effects are negligible in a monolithic cavity), as well as a temperature coupling from the ultra low expansion (ULE) glass, used as a spacer material. This thermal coupling is defined by

$$s_{xx}(f) = \alpha \cdot s_{\text{TT}}(f) \quad (9)$$

where $s_{\text{TT}}(f)$ is the temperature noise, assumed to be $1 \mu\text{K}/\sqrt{\text{Hz}}$ at 1 Hz [53], and the constant of thermal expansion (CTE) α . The CTE according to the manufacturer is $\alpha_{\text{ULE}} = (0 \pm 30) \times 10^{-9} \text{ K}^{-1}$ [54], but to not underestimate the thermal coupling in our

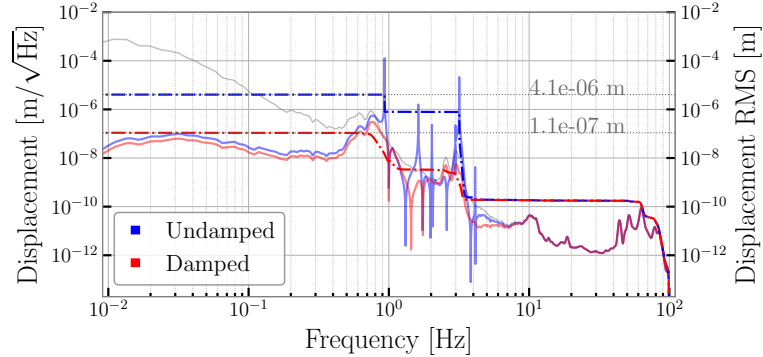


Figure 6. Expected motion spectrum (solid-lines) and RMS motion (dashed-lines) of the top mass with measured seismic motion (grey) as input.

simulation we used a value of 0.1 ppm/K. From here we can take the sum of the before mentioned noise contributions to calculate \tilde{l}_{ref} and \tilde{f} and convert to the displacement noise of the suspended cavity via

$$\tilde{l}_{\text{sus}} = \frac{\tilde{f}}{f_0} \cdot l_{\text{sus}} = \frac{\tilde{l}_{\text{ref}}}{l_{\text{ref}}} \cdot l_{\text{sus}} \quad (10)$$

with the absolute lengths per cavity of $l_{\text{ref}} = 20$ cm and $l_{\text{sus}} = 40$ cm.

4. Simulating noise budget for the current setup

For the calculation of the pendulum motion only inputs in x and pitch DOF were used and taken from the measurement of the optical table motion. Motion in all other DOFs were set to 0, as their coupling to the cavity axis motion (x-direction) is negligible [55].

To estimate an appropriate DAC range, it is essential to know the expected motion at the top mass. The resulting spectrum and the RMS motion of it are presented in Figure 6. By taking the maximum RMS motion of the undamped suspension and performing the calculations from Equation 3 in reverse, we derive a required DAC range for control of ± 0.5 V, which includes a safety margin of a factor of two, thus, the expected noise after the coil driver is attenuated to 1/20 of that which was estimated above.

Since the property of interest in our experiment is the differential motion of the cavity mirrors, we must make an assumption about the extent to which the seismic input couples differently in the two suspensions, specifically regarding how well the mechanical properties can be matched. We assume a coupling of 1%, meaning that 99% of the common seismic motion is rejected. From the resulting time series of the pendulum model, the ASD was calculated using the Daniell averaging method [56], and the contributions from other noise sources were added.

The noise predicted for the cavity length sensing is depicted in Figure 7 and shows only a slight difference at frequencies from 4 Hz to 7 Hz between a damped system that uses BOSEMs (red) for sensing and one that uses COBRIIs (blue). The influence of the BOSEM noise is primarily masked by the ground motion coupling, which dominates at

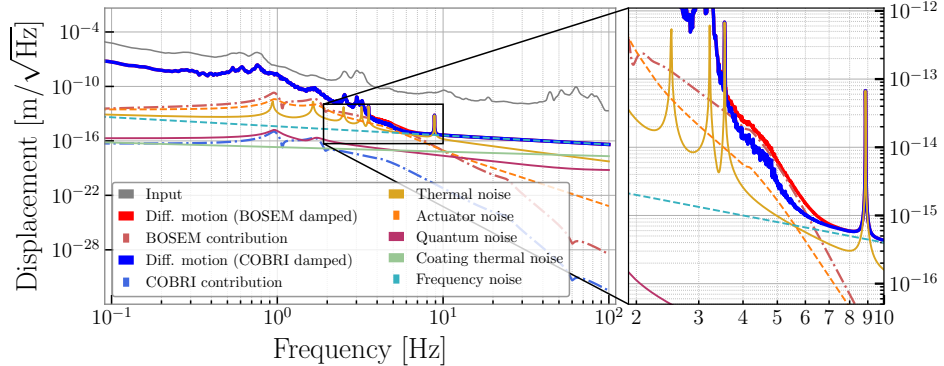


Figure 7. Noise budget of the cavity motion with the cavity constructed between the test-masses. Most important here the difference between the solid red and blue curves indicating the achievable improvement by switching to interferometric sensors.

frequencies below 7 Hz, and at higher frequencies, we are limited by suspension thermal noise. Constructing the cavity between the penultimate masses of the suspensions would increase the coupling to sensor noise, however the coupling to ground motion is increased as well, resulting in a similarly small difference between both damping cases.

But there is also rotational motion to dampen, and in LIGO, the BOSEMs are not used to control rotations [57, 58]. The reason is the large BOSEM self-noise compared to the rotational seismic motion. In our case, the BOSEMs would introduce additional rotational motion to the top mass above 3 Hz, as shown in Figure 8, which exceeds the existing rotational motion on the optical table. This makes it infeasible to use BOSEMs to dampen any rotations, not just for pitch. On the other hand, local interferometric sensors have a much lower self-noise, which lies well beneath the measured rotational motion, making them advantageous for controlling rotations, as demonstrated in ref [32].

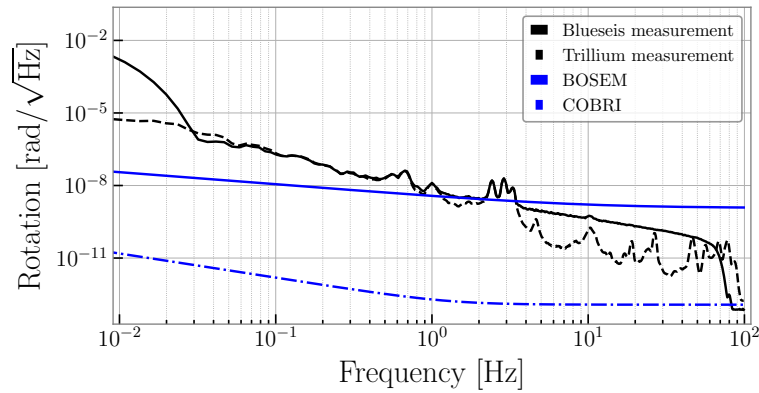


Figure 8. Measured pitch motion compared to BOSEM and COBRI pitch noise on the HRTS.

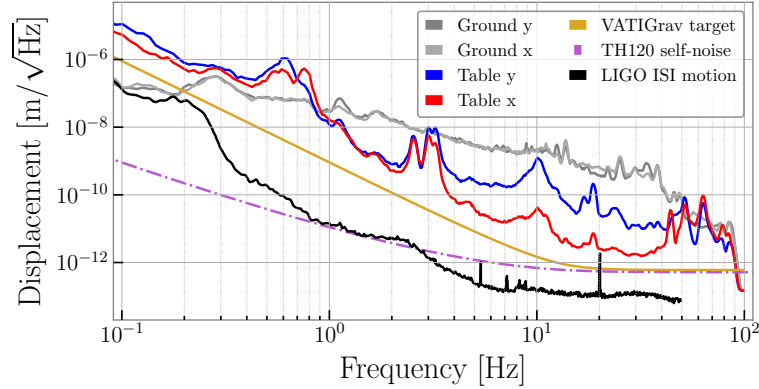


Figure 9. Target for future seismic motion on the optical table (yellow) in comparison to the current motion (blue & red) and motion of the LIGO ISI (black)

5. Tightening seismic isolation requirements

To achieve a larger margin between a BOSEM- and a COBRI-damped pendulum, the seismic isolation of the optical table needs to be improved, which would reduce the RMS motion, specifically of the top mass, thus increasing the difference of the two damping cases. The reduced RMS motion additionally allows us to further reduce the DAC range and therefore the actuator noise.

We created a target spectrum based on our current measurements, compared to the LIGO ISI [59, 60] motion at the suspension point of one of the input test masses [61] and the self-noise of the TH120 [62]. The TH120 will later be used on the optical table to create a feedback loop in conjunction with the active isolation feet of the chamber. The result, shown in Figure 9, consists of a f^{-3} slope at low frequencies and is flat at high frequencies due to the self-noise of the TH120. Our general aim is to improve isolation by one to two orders of magnitude, depending on frequency. This positions the target spectrum between the LIGO ISI noise and our current performance.

Feeding the seismic noise target into the suspension model results in a decrease in

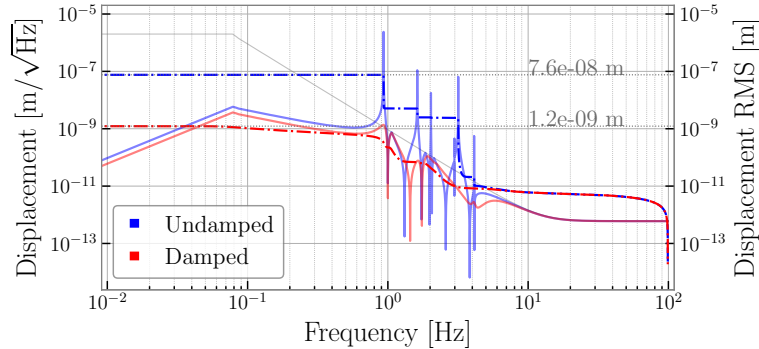


Figure 10. Expected motion spectrum (solid-lines) and RMS motion (dashed-lines) of the top mass with seismic target (grey) as input

the RMS motion by roughly two orders of magnitude, as shown in Figure 10. This is mainly due to the absence of resonances of the passive and active isolation in the target noise, which are difficult to predict and are expected to be reduced after improving the isolation. This improvement would theoretically allow us to reduce the DAC range by two orders of magnitude; however, we would be limited by the noise of the Analogue-to-Digital Converters (ADC), used for BOSEM readout, at roughly $3 \times 10^{-7} \text{ V}/\sqrt{\text{Hz}}$. We therefore assume a conservative reduction in the DAC range by one order of magnitude.

The effect on the differential motion is depicted in Figure 11. The difference between the BOSEM- and COBRI-controlled systems increased significantly, providing a large margin to demonstrate the advantages of COBRIs over BOSEMs in terms of sensitivity and suspension damping of at least an order of magnitude.

The seismic pre-isolation improvement that we aim for will be achieved by exchanging the inertial sensors in the commercial active isolators, with a set of three Trillium Horizon 120 that we will position on top of the vacuum chamber (for details see ref. [27]) to enable a LIGO ISI-like active control. Additionally, the tuning of the passive dampers and the mass distribution in the passive isolation can be improved further by more careful mechanical tuning, since we do not yet achieve the nominal resonance frequencies.

6. Possible updates to suspension mechanics

Future revisions of this experiment will feature suspensions specifically designed to test high-sensitivity interferometric local displacement sensors. These suspensions must achieve a stronger coupling between sensor noise and test-mass motion without sacrificing seismic isolation. Therefore, reducing the number of pendulum stages or actuating directly on the test mass is not feasible. As stated in [9, 10, 63], high coupling to the actuators can be achieved by using four wires from the mass where the actuation occurs to the test mass, by matching the masses and moments of inertia of each mass,

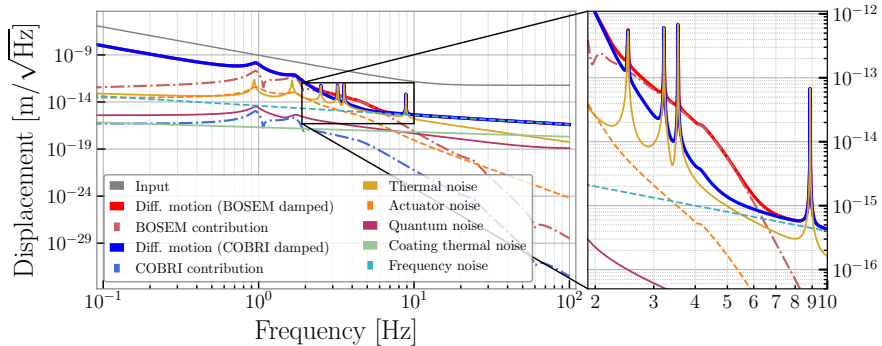


Figure 11. Target noise budget of the cavity motion with the cavity constructed between the test-masses. Most important here the difference between the solid red and blue curves indicating the achievable improvement by switching to interferometric sensors.

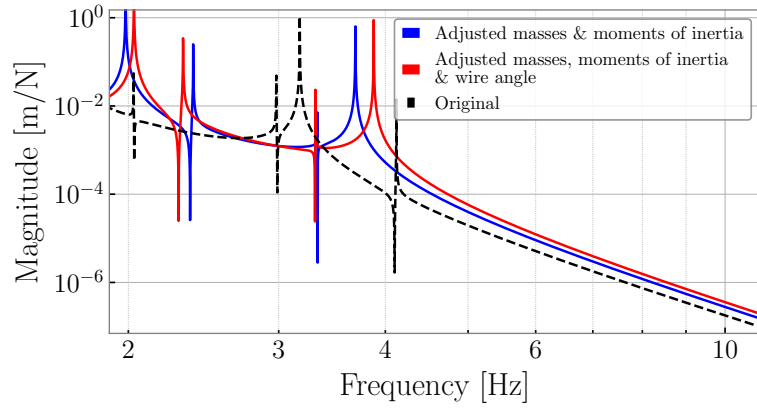


Figure 12. Susceptibility from top mass to test-mass for the original and adjusted mechanics of the HRTS.

and by tuning the angle at which the wire connects to each mass. Figure 12 shows the susceptibility from the top mass to the test mass, indicating the strength of coupling between sensor noise and test-mass motion for the original system and two systems with adjusted mechanical designs. For the blue curve, matching the masses and moments of inertia resulted in an increased coupling by a factor of two over the relevant frequency range of 3–10 Hz. By increasing the angle between the wire and the attachment points at the top, penultimate, and test masses, coupling was further increased, as visualized by the red curve. Therefore, designing a suspension with higher coupling to sensor noise should be achievable with minimal adjustments to existing designs.

7. Conclusion

In this paper we presented the setup and simulation results of an experiment, which aims to directly measure the reduction of controls noise in mirror suspensions using high sensitive interferometric local displacement sensors.

We found that with the current state of our seismic pre-isolation we expect to measure a difference between a system that uses BOSEM and one that uses the COBRI for sensing of up to a factor of two in length stability between 3.5–7 Hz along the cavity axis. By improving our seismic pre-isolation, we should be able to definitively demonstrate the improvements that our COBRI will provide for suspension control over the currently used BOSEM by a factor of 10. In terms of the rotational degrees of freedom (DOFs), measuring the improvement will be straightforward due to BOSEM noise dominating rotational motion in the suspension. Generally, this setup could be used to test any new interferometric displacement sensor, not just the COBRI. The final setup will feature control of all 6 DOFs with BOSEM and COBRI even though the focus of this manuscript was on the cavity axis. Furthermore, realizing this experiment in our environment, including the control system, we can provide a robust case for its implementation in actual observatories. While the full displacement noise improvements

of local sensors will not be directly demonstrated in these experiments, they can in the future be adapted with new, more aggressive damping controllers to reduce also the RMS motion further while retaining suitable in-band noise contributions.

The experiment could in principle benefit from another suspension design where coupling between the sensor noise and the optic would be enhanced. However, creating a new suspension for this purpose would require significant resources and research & development. But with the HRTS we benefit from a well-tested design and a lot of existing expertise, including available mathematical models. Additionally, proving the advantages of using existing LIGO-style suspensions would underscore the improvements that our technology could bring to LIGO or future detectors. Nonetheless, we have shown that designing such a suspension is possible by adjusting a few key parameters of the mechanical design.

While procurement of the major parts of the experiment has been concluded, several parts still require assembly, commissioning and, surely, noise hunting, with first major results expected by mid of 2026.

Data availability statement

All data that support the findings of this study are included within the article (and any supplementary files).

Acknowledgments

The authors thank Mark Barton for providing the Mathematica models and our colleagues from ET-Pathfinder, especially Joris van Heijningen and Stephan Hild, for us being able to borrow the HRTSs. Furthermore we want to thank Jan-Niklas Feldhusen for assisting with the assembly of the HRTSs, Johannes Lehmann for the scientific exchange on the optical setup, the SWG (seismic working group) team from LIGO for useful discussions, Conor Mow-Lowry for his helpful comments throughout the creation of this manuscript, and Jeffrey Kissel for providing the control filters. We acknowledge funding by the Bundesministerium für Bildung und Forschung (BMBF) under project references 05A20GU5 & 05A23GU5 and by the Deutsche Forschungsgemeinschaft (DFG, German Research Foundation) under Germany’s Excellence Strategy—EXC 2121 “Quantum Universe”—390833306.

References

- [1] LIGO Scientific and Virgo Collaborations et al. “The basic physics of the binary black hole merger GW150914”. In: *Annalen der Physik* 529.1 (Jan. 2017), p. 1600209. ISSN: 0003-3804, 1521-3889. DOI: 10.1002/andp.201600209. URL: <https://onlinelibrary.wiley.com/doi/10.1002/andp.201600209> (visited on 02/05/2024).
- [2] J. Aasi et al. “Advanced LIGO”. In: *Classical and Quantum Gravity* 32.7 (Mar. 2015). Publisher: IOP Publishing, p. 074001. ISSN: 0264-9381. DOI: 10.1088/0264-9381/32/7/074001. URL: <https://doi.org/10.1088/0264-9381/32/7/074001> (visited on 05/30/2021).

- [3] The LIGO Scientific Collaboration et al. “GWTC-2.1: Deep Extended Catalog of Compact Binary Coalescences Observed by LIGO and Virgo During the First Half of the Third Observing Run”. In: *arXiv:2108.01045 [gr-qc]* (Aug. 2, 2021). arXiv: 2108.01045. URL: <http://arxiv.org/abs/2108.01045> (visited on 10/22/2021).
- [4] Virgo Collaboration LIGO Scientific Collaboration {and} KAGRA Collaboration et al. “GWTC-3: Compact Binary Coalescences Observed by LIGO and Virgo during the Second Part of the Third Observing Run”. In: *Physical Review X* 13.4 (Dec. 4, 2023). Publisher: American Physical Society, p. 041039. DOI: 10.1103/PhysRevX.13.041039. URL: <https://link.aps.org/doi/10.1103/PhysRevX.13.041039>.
- [5] B. P. Abbott et al. “Prospects for observing and localizing gravitational-wave transients with Advanced LIGO, Advanced Virgo and KAGRA”. In: *Living Reviews in Relativity* 23.1 (Dec. 2020), p. 3. ISSN: 2367-3613, 1433-8351. DOI: 10.1007/s41114-020-00026-9. URL: <https://link.springer.com/10.1007/s41114-020-00026-9> (visited on 05/23/2023).
- [6] F. Acernese et al. “Advanced Virgo: a second-generation interferometric gravitational wave detector”. In: *Classical and Quantum Gravity* 32.2 (Jan. 22, 2015), p. 024001. ISSN: 0264-9381, 1361-6382. DOI: 10.1088/0264-9381/32/2/024001. URL: <https://iopscience.iop.org/article/10.1088/0264-9381/32/2/024001> (visited on 12/05/2023).
- [7] T. Akutsu et al. “Overview of KAGRA: Detector design and construction history”. In: *Progress of Theoretical and Experimental Physics* 2021.5 (May 1, 2021). ISSN: 2050-3911. DOI: 10.1093/ptep/ptaa125. URL: <https://doi.org/10.1093/ptep/ptaa125> (visited on 06/13/2021).
- [8] B. P. Abbott et al. “Multi-messenger Observations of a Binary Neutron Star Merger”. In: *The Astrophysical Journal Letters* 848.2 (Oct. 20, 2017), p. L12. ISSN: 2041-8205, 2041-8213. DOI: 10.3847/2041-8213/aa91c9. URL: <https://iopscience.iop.org/article/10.3847/2041-8213/aa91c9>.
- [9] N. A. Robertson et al. “Quadruple suspension design for Advanced LIGO”. In: *Classical and Quantum Gravity* 19.15 (July 2002), pp. 4043–4058. ISSN: 0264-9381. DOI: 10.1088/0264-9381/19/15/311. URL: <https://doi.org/10.1088/0264-9381/19/15/311> (visited on 02/26/2020).
- [10] K. A. Strain and B. N. Shapiro. “Damping and local control of mirror suspensions for laser interferometric gravitational wave detectors”. In: *Review of Scientific Instruments* 83.4 (Apr. 1, 2012), p. 044501. ISSN: 0034-6748. DOI: 10.1063/1.4704459. URL: <https://aip.scitation.org/doi/10.1063/1.4704459> (visited on 06/30/2019).
- [11] L. Carbone et al. “Sensors and actuators for the Advanced LIGO mirror suspensions”. In: *Classical and Quantum Gravity* 29.11 (2012). tex.ids= Carbone2012a, carbone2012a publisher: IOP Publishing, p. 115005. URL: <http://stacks.iop.org/0264-9381/29/i=11/a=115005>.
- [12] Tomotada Akutsu et al. “Compact integrated optical sensors and electromagnetic actuators for vibration isolation systems in the gravitational-wave detector KAGRA”. In: *Review of Scientific Instruments* 91.11 (Nov. 1, 2020). Publisher: American Institute of Physics, p. 115001. ISSN: 0034-6748. DOI: 10.1063/5.0022242. URL: <https://aip.scitation.org/doi/full/10.1063/5.0022242> (visited on 01/02/2021).
- [13] S J Cooper et al. “Sensors and Actuators for the Advanced LIGO+ Upgrade”. In: *AIP* (2022). DOI: 10.48550/ARXIV.2208.00798. URL: <https://arxiv.org/abs/2208.00798>.
- [14] E. Capote et al. “Advanced LIGO detector performance in the fourth observing run”. In: *Physical Review D* 111.6 (Mar. 3, 2025). Publisher: American Physical Society, p. 062002. DOI: 10.1103/PhysRevD.111.062002. URL: <https://link.aps.org/doi/10.1103/PhysRevD.111.062002> (visited on 04/22/2025).
- [15] S. J. Cooper et al. “A compact, large-range interferometer for precision measurement and inertial sensing”. In: *Classical and Quantum Gravity* 35.9 (Mar. 2018), p. 095007. ISSN: 0264-9381. DOI: 10.1088/1361-6382/aab2e9. URL: <https://doi.org/10.1088/0264-9381/35/9/095007>.

- [16] J. van Dongen et al. “Reducing controls noise in gravitational wave detectors with interferometric local damping of suspended optics”. In: (May 2, 2023). DOI: 10.48550/arXiv.2205.01434. arXiv: 2205.01434. URL: <http://arxiv.org/abs/2205.01434> (visited on 11/18/2024).
- [17] David Reitze et al. *Cosmic Explorer: The U.S. Contribution to Gravitational-Wave Astronomy beyond LIGO*. July 10, 2019. DOI: 10.48550/arXiv.1907.04833. URL: <http://arxiv.org/abs/1907.04833> (visited on 11/05/2024).
- [18] M Punturo et al. “The Einstein Telescope: a third-generation gravitational wave observatory”. In: *Classical and Quantum Gravity* 27.19 (2010), p. 194002. URL: https://hal.archives-ouvertes.fr/hal-00629986/file/PEER_stage2_10.1088%252F0264-9381%252F27%252F19%252F194002.pdf.
- [19] Adrian Abac et al. *The Science of the Einstein Telescope*. Mar. 15, 2025. DOI: 10.48550/arXiv.2503.12263. arXiv: 2503.12263[gr-qc]. URL: <http://arxiv.org/abs/2503.12263> (visited on 04/22/2025).
- [20] Oliver Gerberding and Katharina-Sophie Isleif. “Ghost Beam Suppression in Deep Frequency Modulation Interferometry for Compact On-Axis Optical Heads”. In: *Sensors* 21.5 (Jan. 2021). Number: 5 Publisher: Multidisciplinary Digital Publishing Institute, p. 1708. DOI: 10.3390/s21051708. URL: <https://www.mdpi.com/1424-8220/21/5/1708>.
- [21] Oliver Gerberding. “Deep frequency modulation interferometry”. In: *Optics Express* 23.11 (2015). tex.ids: gerberding2015c, pp. 14753–14762. DOI: 10.1364/OE.23.014753. URL: <https://www.osapublishing.org/oe/abstract.cfm?uri=oe-23-11-14753>.
- [22] Adam Huddart. “HRTS Final Design Document”. In: *LIGO Document Control Center* LIGO-T2000670-v3 (Nov. 13, 2020). URL: <https://dcc.ligo.org/LIGO-T2000670>.
- [23] Peter Fritschel, Matthew Evans, and Valery Frolov. “Balanced homodyne readout for quantum limited gravitational wave detectors”. In: *Optics Express* 22.4 (Feb. 24, 2014). Publisher: Optica Publishing Group, pp. 4224–4234. ISSN: 1094-4087. DOI: 10.1364/OE.22.004224. URL: <https://opg.optica.org/oe/abstract.cfm?uri=oe-22-4-4224> (visited on 07/26/2022).
- [24] M Barton et al. “Preliminary Design: Balanced Homodyne Detection for A+”. In: *LIGO Document Control Center* LIGO-T2000581 (Aug. 21, 2024). URL: <https://dcc.ligo.org/LIGO-T2000581>.
- [25] A Utina et al. “ETpathfinder: a cryogenic testbed for interferometric gravitational-wave detectors”. In: *Classical and Quantum Gravity* 39.21 (Sept. 2022). Publisher: IOP Publishing, p. 215008. ISSN: 0264-9381. DOI: 10.1088/1361-6382/ac8fdb. URL: <https://dx.doi.org/10.1088/1361-6382/ac8fdb> (visited on 04/22/2025).
- [26] Stuart Aston. “BOSEM Design Document & Test Report”. In: *LIGO Document Control Center* LIGO-T050111-v6 (Feb. 2014). tex.ids= aston2014. URL: <https://dcc.ligo.org/LIGO-T050111/public>.
- [27] Artem Basalaev, Jan-Niklas Feldhusen, and Oliver Gerberding. *Characterizing seismic isolation using convolutional neural networks and Wiener filters*. Oct. 18, 2024. DOI: 10.48550/arXiv.2410.14806. arXiv: 2410.14806. URL: <http://arxiv.org/abs/2410.14806> (visited on 10/22/2024).
- [28] R. W. P. Drever et al. “Laser phase and frequency stabilization using an optical resonator”. In: *Applied Physics B Photophysics and Laser Chemistry* 31.2 (June 1983), pp. 97–105. ISSN: 0721-7269, 1432-0649. DOI: 10.1007/BF00702605. URL: <http://link.springer.com/10.1007/BF00702605> (visited on 10/14/2021).
- [29] LIGO Scientific Collaboration. *CDS · GitLab*. GitLab. Mar. 14, 2025. URL: <https://git.ligo.org/cds> (visited on 04/28/2025).
- [30] Yichao Yang et al. “Single-Element Dual-Interferometer for Precision Inertial Sensing”. In: *Sensors* 20.17 (Sept. 2020), p. 4986. ISSN: 1424-8220. DOI: 10.3390/s20174986. URL: <https://dx.doi.org/10.3390/s20174986>.

- [31] Jiri Smetana et al. “Compact Michelson Interferometers with Subpicometer Sensitivity”. In: *Phys. Rev. Appl.* 18 (3 Sept. 2022), p. 034040. DOI: 10.1103/PhysRevApplied.18.034040. URL: <https://link.aps.org/doi/10.1103/PhysRevApplied.18.034040>.
- [32] Alexandra Mitchell et al. *Integration of high-performance compact interferometric sensors in a suspended interferometer*. 2024. DOI: 10.48550/ARXIV.2409.08843. URL: <https://arxiv.org/abs/2409.08843>.
- [33] Mark Barton. “Models of the Advanced LIGO Suspensions in Mathematica™”. In: *LIGO Document Control Center* LIGO-T020205 (Apr. 28, 2014). URL: <https://dcc.ligo.org/LIGO-T020205>.
- [34] Artem Basalaev et al. *Spicypy*. Version v0.8. Oct. 2024. DOI: 10.5281/zenodo.10033637. URL: <https://doi.org/10.5281/zenodo.10033637>.
- [35] Sawyer Fuller et al. “The Python Control Systems Library (python-control)”. In: *60th IEEE Conference on Decision and Control (CDC)*. IEEE. 2021, pp. 4875–4881.
- [36] D. M. Macleod et al. “GWpy: A Python package for gravitational-wave astrophysics”. In: *SoftwareX* 13 (2021), p. 100657. ISSN: 2352-7110. DOI: 10.1016/j.softx.2021.100657. URL: <https://www.sciencedirect.com/science/article/pii/S2352711021000029>.
- [37] Michael Tröbs and Gerhard Heinzel. “Improved spectrum estimation from digitized time series on a logarithmic frequency axis”. In: *Measurement* 39.2 (2006), pp. 120–129. ISSN: 0263-2241. DOI: <https://doi.org/10.1016/j.measurement.2005.10.010>. URL: <https://www.sciencedirect.com/science/article/pii/S026322410500117X>.
- [38] Martin Hewitson. *LTPDA: a MATLAB toolbox for accountable and reproducible data analysis*. <https://www.lisamission.org/ltpda/>. Online; accessed 2024-08-15. 2024.
- [39] Jeffrey Kissel. *x1suslo1 (HRTS) and x1susbs (BBSS) Controls Ready for Suspension Testing*. aLIGO LHO Logbook. URL: <https://alog.ligo-wa.caltech.edu/aLOG/index.php?callRep=74142> (visited on 11/05/2024).
- [40] Sander K. Sijtsma et al. *Non-Smooth Multi-objective Controller Synthesis for Test-Mass Actuation in Gravitational-Wave Detectors*. 2025. DOI: 10.48550/ARXIV.2504.05100. URL: <https://arxiv.org/abs/2504.05100>.
- [41] Stuart Aston. “Advanced LIGO BOSEM Noise Measurement Report”. In: *LIGO Document Control Center* LIGO-T0900496 (Mar. 21, 2011). URL: <https://dcc.ligo.org/LIGO-T0900496>.
- [42] Tobias Eckhardt and Oliver Gerberding. “Noise Limitations in Multi-Fringe Readout of Laser Interferometers and Resonators”. In: *Metrology* 2.1 (Mar. 2022). Number: 1 Publisher: Multidisciplinary Digital Publishing Institute, pp. 98–113. ISSN: 2673-8244. DOI: 10.3390/metrology2010007. URL: <https://www.mdpi.com/2673-8244/2/1/7> (visited on 10/30/2022).
- [43] Oliver Gerberding et al. “Laser-Frequency Stabilization via a Quasimonolithic Mach-Zehnder Interferometer with Arms of Unequal Length and Balanced dc Readout”. In: *Physical Review Applied* 7.2 (Feb. 2017). ISSN: 2331-7019. DOI: 10.1103/physrevapplied.7.024027. URL: <http://dx.doi.org/10.1103/PhysRevApplied.7.024027>.
- [44] Katharina-Sophie Isleif et al. “Compact Multifringe Interferometry with Subpicometer Precision”. In: *Phys. Rev. Appl.* 12 (3 Sept. 2019), p. 034025. DOI: 10.1103/PhysRevApplied.12.034025. URL: <https://link.aps.org/doi/10.1103/PhysRevApplied.12.034025>.
- [45] *Trillium Horizon 120 — Nanometrics*. URL: <https://nanometrics.ca/instrumentation/products/seismometers/trillium-horizon-120> (visited on 11/05/2024).
- [46] Gizem Izgi et al. “Performance Test of the Rotational Sensor blueSeis-3A in a Huddle Test in Fürstenfeldbruck”. In: *Sensors* 21.9 (Jan. 2021). Number: 9 Publisher: Multidisciplinary Digital Publishing Institute, p. 3170. ISSN: 1424-8220. DOI: 10.3390/s21093170. URL: <https://www.mdpi.com/1424-8220/21/9/3170> (visited on 05/10/2022).

[47] Gabriela González. “Suspensions Thermal Noise in the LIGO Gravitational Wave Detector”. In: *arXiv:gr-qc/0006053* (June 30, 2000). doi: 10.1088/0264-9381/17/21/305. arXiv: gr-qc/0006053. URL: <http://arxiv.org/abs/gr-qc/0006053> (visited on 10/16/2020).

[48] Francesco Piergiovanni, Michele Punturo, and P Puppo. “The thermal noise of the Virgo+ and Virgo Advanced Last Stage Suspension (The PPP effect)”. In: *Virgo TDS VIR-0015E-09* (Sept. 12, 2009), p. 27. URL: <https://tds.virgo-gw.eu/?content=3&r=7233> (visited on 11/13/2024).

[49] William Yam, Slawek Gras, and Matthew Evans. “Multimaterial coatings with reduced thermal noise”. In: *Physical Review D* 91.4 (Feb. 2015). ISSN: 1550-2368. doi: 10.1103/physrevd.91.042002. URL: <http://dx.doi.org/10.1103/PhysRevD.91.042002>.

[50] Simon C. Tait et al. “Demonstration of the Multimaterial Coating Concept to Reduce Thermal Noise in Gravitational-Wave Detectors”. In: *Physical Review Letters* 125.1 (July 2020). ISSN: 1079-7114. doi: 10.1103/physrevlett.125.011102. URL: <http://dx.doi.org/10.1103/PhysRevLett.125.011102>.

[51] <https://media.schott.com/api/public/content/41e799d0bf874807a0bb8e702fbb75b5?v=54856406>. [Accessed 30-04-2025].

[52] Eric D. Black. “An introduction to Pound–Drever–Hall laser frequency stabilization”. In: *American Journal of Physics* 69.1 (Jan. 1, 2001), pp. 79–87. ISSN: 0002-9505, 1943-2909. doi: 10.1119/1.1286663. URL: <https://pubs.aip.org/ajp/article/69/1/79/1055569/An-introduction-to-Pound-Drever-Hall-laser>.

[53] David Roma-Dollase et al. “Resistive-Based Micro-Kelvin Temperature Resolution for Ultra-Stable Space Experiments”. In: *Sensors* 23.1 (Jan. 2023). Number: 1 Publisher: Multidisciplinary Digital Publishing Institute, p. 145. ISSN: 1424-8220. doi: 10.3390/s23010145. URL: <https://www.mdpi.com/1424-8220/23/1/145> (visited on 12/30/2022).

[54] *Ultra-Low Expansion Glass — Low CTE Glass — Corning*. URL: <https://www.corning.com/worldwide/en/products/advanced-optics/product-materials/semiconductor-laser-optic-components/ultra-low-expansion-glass.html> (visited on 04/30/2025).

[55] M Barton. *sus - Revision 12079: / trunk / Common / MathematicaModels / TripleLite2 / mark.barton / 20210824hrts0*. URL: <https://svn.ligo.caltech.edu/svn/sus/trunk/Common/MathematicaModels/TripleLite2/mark.barton/20210824hrts0/> (visited on 11/18/2024).

[56] Aleksander Labuda. “Daniell method for power spectral density estimation in atomic force microscopy”. In: *Review of Scientific Instruments* 87.3 (Mar. 2016), p. 033704. ISSN: 0034-6748. doi: 10.1063/1.4943292. eprint: <https://pubs.aip.org/aip/rsi/article-pdf/doi/10.1063/1.4943292/14918509/033704_1_online.pdf>. URL: <https://doi.org/10.1063/1.4943292>.

[57] D. H. Shoemaker and J. H. Tappan. “Alignment Sensing/Control (ASC) Optical Lever Specification and Design Document”. In: *LIGO Document Control Center* LIGO-T950112 (Feb. 10, 1996). URL: <https://dcc.ligo.org/LIGO-T950112> (visited on 11/18/2024).

[58] Eric D Black et al. “Advanced-LIGO Optical Levers Design Requirements”. In: *LIGO Document Control Center* LIGO-T0900174-v2 (Mar. 26, 2010). URL: <https://dcc.ligo.org/LIGO-T0900174>.

[59] Fabrice Matichard et al. *Advanced LIGO Two-Stage Twelve-Axis Vibration Isolation and Positioning Platform. Part 1: Design and Production Overview*. July 23, 2014. doi: 10.48550/arXiv.1407.6377. arXiv: 1407.6377. URL: <http://arxiv.org/abs/1407.6377> (visited on 11/18/2024).

[60] Fabrice Matichard et al. *Advanced LIGO Two-Stage Twelve-Axis Vibration Isolation and Positioning Platform. Part 2: Experimental Investigation and Tests Results*. July 23, 2014. doi: 10.48550/arXiv.1407.6324. arXiv: 1407.6324. URL: <http://arxiv.org/abs/1407.6324> (visited on 11/18/2024).

- [61] Brian Lantz. “ISI motion targets for A# calculations”. Nov. 28, 2023. URL: https://dcc.ligo.org/DocDB/0190/G2302230/001/G2302230_BSC_req_slides.pdf (visited on 11/05/2024).
- [62] J S Kissel. *LIGO / SVN / seismic / common / MatlabTools*. June 11, 2025. URL: <https://svn.ligo.caltech.edu/svn/seismic/Common/MatlabTools/> (visited on 06/11/2025).
- [63] M. V. Plissi et al. “GEO 600 triple pendulum suspension system: Seismic isolation and control”. In: *Review of Scientific Instruments* 71.6 (June 2000). tex.ids: plissi2000a, pp. 2539–2545. ISSN: 0034-6748, 1089-7623. DOI: 10.1063/1.1150645. URL: <http://aip.scitation.org/doi/10.1063/1.1150645> (visited on 03/23/2020).